

# Structure-Based Discovery of a Novel Allosteric Inhibitor against Human Dopamine Transporter

Shengzhe Deng, Haiwei Zhang,\* Rongpei Gou, Ding Luo, Zerong Liu, Feng Zhu, and Weiwei Xue\*



Cite This: *J. Chem. Inf. Model.* 2023, 63, 4458–4467



Read Online

ACCESS |



Metrics & More

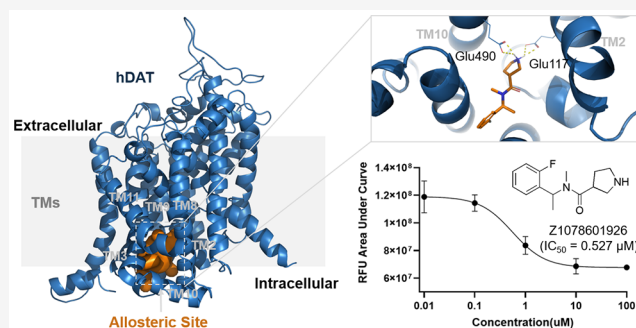


Article Recommendations



Supporting Information

**ABSTRACT:** Human dopamine transporter (hDAT) regulates the reuptake of extracellular dopamine (DA) and is an essential therapeutic target for central nervous system (CNS) diseases. The allosteric modulation of hDAT has been identified for decades. However, the molecular mechanism underlying the transportation is still elusive, which hinders the rational design of allosteric modulators against hDAT. Here, a systematic structure-based method was performed to explore allosteric sites on hDAT in inward-open (IO) conformation and to screen compounds with allosteric affinity. First, the model of the hDAT structure was constructed based on the recently reported Cryo-EM structure of the human serotonin transporter (hSERT) and Gaussian-accelerated molecular dynamics (GaMD) simulation was further utilized for the identification of intermediate energetic stable states of the transporter. Then, with the potential druggable allosteric site on hDAT in IO conformation, virtual screening of seven enamine chemical libraries (~440,000 compounds) was processed, resulting in 10 compounds being purchased for *in vitro* assay and with Z1078601926 discovered to allosterically inhibit hDAT ( $IC_{50} = 0.527 [0.284; 0.988] \mu\text{M}$ ) when nomifensine was introduced as an orthosteric ligand. Finally, the synergistic effect underlying the allosteric inhibition of hDAT by Z1078601926 and nomifensine was explored using additional GaMD simulation and postbinding free energy analysis. The hit compound discovered in this work not only provides a good starting point for lead optimization but also demonstrates the usability of the method for the structure-based discovery of novel allosteric modulators of other therapeutic targets.



## INTRODUCTION

Dopamine transporter (DAT) is a member of the solute carrier 6 (SLC6) family belonging to the larger family of neurotransmitter sodium symporters (NSSs).<sup>1</sup> DAT functions by recycling dopamine (DA) from the synaptic cleft into presynaptic neurons, which reduces the activity in the dopaminergic system.<sup>2</sup> The dysregulation of DAT is considered to be related to psychiatric disorders such as depression, attention deficit hyperactivity disorder (ADHD), and Parkinson's disease (PD).<sup>3,4</sup> Moreover, drug abuse of cocaine and methamphetamine, which is a widely concerned issue of public health, is also caused by the dysfunction of DAT.<sup>5</sup> Therefore, DAT is regarded as an essential therapeutic target of central nervous system (CNS) diseases.<sup>6</sup>

Nowadays, the structural knowledge of DAT is still based on the studies of homogeneous NSSs including leucine transporter (LeuT),<sup>7</sup> *Drosophila melanogaster* dopamine transporter (dDAT),<sup>8</sup> and human serotonin transporter (hSERT).<sup>9</sup> Resembling the first published NSS structure of LeuT,<sup>7</sup> DAT is composed of 12  $\alpha$ -helical transmembrane domains (TMs) connected by intracellular and extracellular loops (ILs and ELs), and 10 TMs (TM1–TM5 and TM6–TM10) are organized into two inverted-topological repeats. DAT binds DA or other neurotransmitters in the primary substrate

binding site (S1), also defined as the orthosteric site.<sup>10</sup> A circulation of conformational alterations exists in the process of DA's translocation, including outward-open (OO), occluded (OC), and inward-open (IO) conformations.<sup>11</sup>

The conventional drugs targeting DAT, such as dopamine reuptake inhibitor (DRI), act as competitive inhibitors, which occupy the orthosteric site.<sup>8,12,13</sup> The allosteric modulation of hDAT has been identified for decades,<sup>14</sup> and recently the allosteric (S2) site near the orthosteric one has also been identified in DAT<sup>15</sup> and other NSSs, including LeuT<sup>16</sup> and serotonin transporter (SERT),<sup>17–19</sup> which is mainly located at the periphery of the ELs region.<sup>20</sup> Nevertheless, allosteric sites are generally less conservative and could exist among a vast range of residues, which makes allosteric drug discovery of DAT both promising and cryptic work.<sup>10,12</sup>

Received: March 26, 2023

Published: July 6, 2023



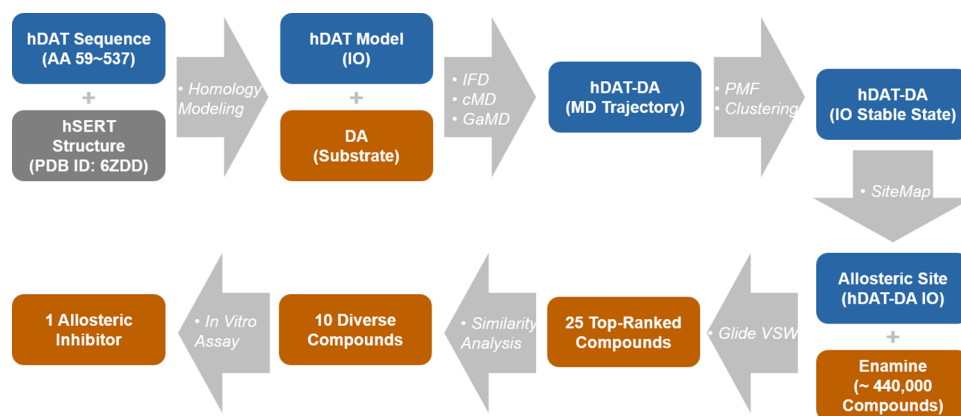


**Figure 1.** Brief workflow describes the structure-based discovery of a novel allosteric inhibitor against hDAT. First, a model of hDAT in IO conformation was constructed by MODELLER using hSERT (PDB ID: 6ZDD) as a template and submitted for optimization by MD simulations. Then, two-dimensional (2D)-PMF and clustering analysis were used to characterize the stable IO conformation of hDAT. The allosteric sites were predicted by SiteMap and used for Glide virtual screening of the enamine chemical library (~440,000 compounds). Finally, through chemical similarity analysis, 10 compounds with diverse scaffolds were selected from the 25 top-ranking compounds and purchased for *in vitro* inhibition assay.

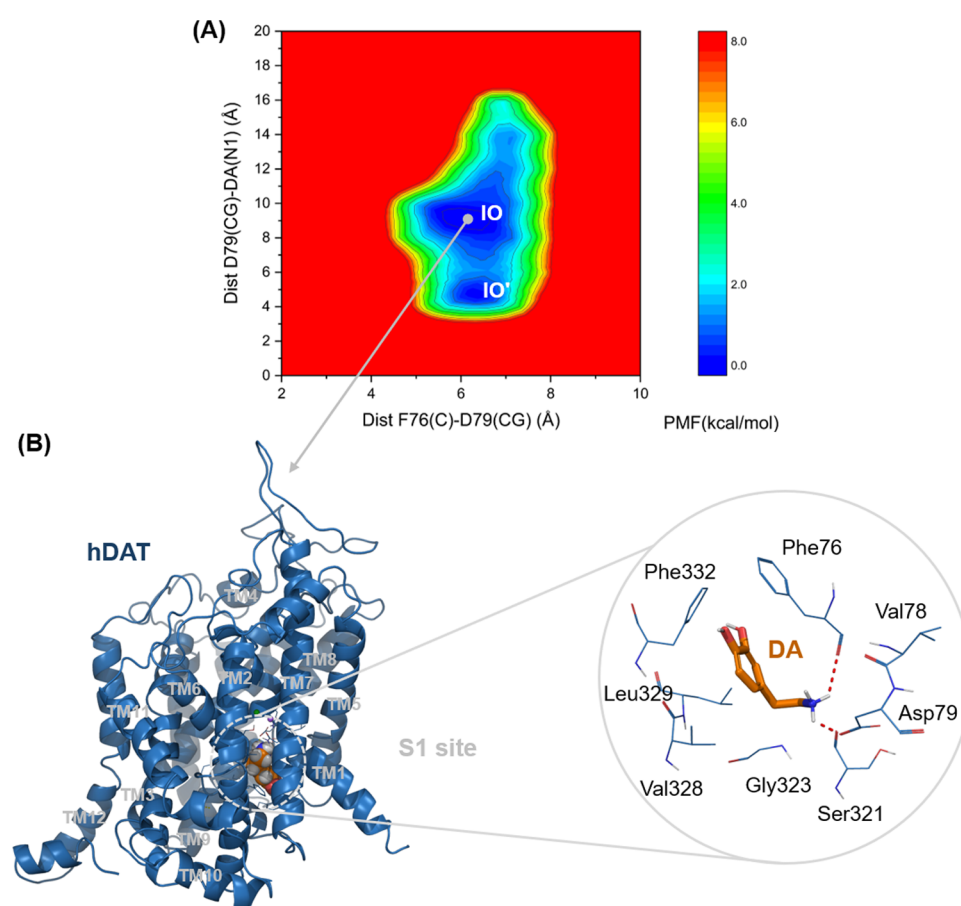


**Figure 2.** Structure and free energy landscape of DA in complex with IO hDAT. (A) 2D potential of mean force (PMF) profile of DA in complex with IO hDAT, regarding the distances between the  $C_{\beta}$  of Phe76-the  $C_{\gamma}$  of Asp79 and the  $C_{\gamma}$  of Asp79-the  $N_1$  of DA. Two energetic wells were centered at (6.0, 9.1 Å) and (6.3, 4.7 Å). (B) Representative snapshot of the complex in the low-energy well (left) and the binding mode between DA and hDAT.

The present study aims to explore alternative allosteric binding sites of human DAT (hDAT), especially in a certain conformational state of hDAT and with orthosteric substrate binding. Based on the crystal structure of hSERT, a homology model of the DA-bound hDAT in IO conformation was constructed and optimized by Gaussian-accelerated molecular

dynamics (GaMD) simulation. The equilibrium state of the model was characterized through free energy landscape analysis of potentials of mean force (PMF). A new druggable allosteric site located at the intracellular domain was identified and used for virtual screening and *in vitro* assay, resulting in the discovery of the compound Z1078601926 as a novel allosteric

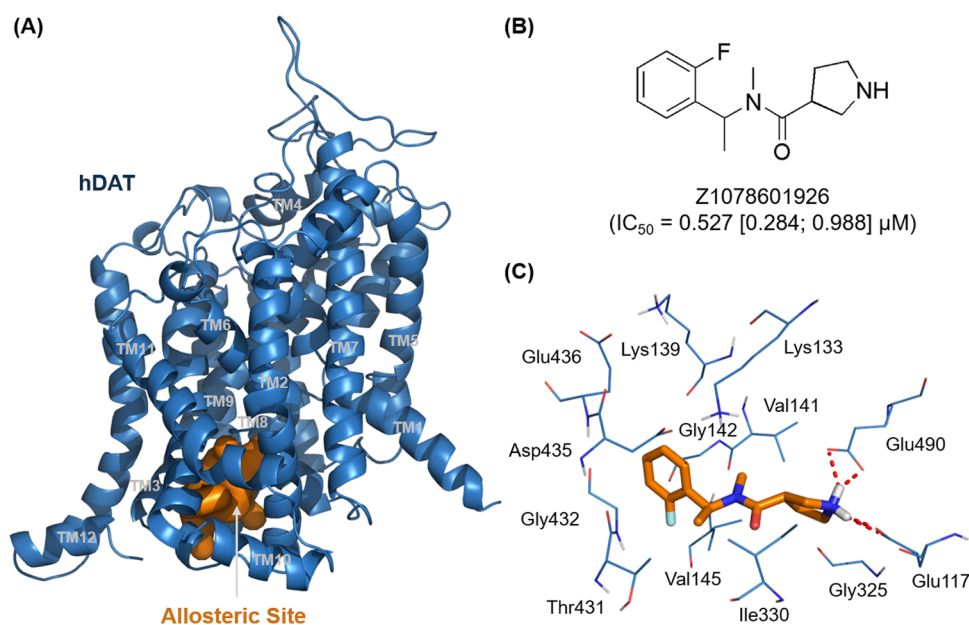


**Figure 3.** Allosteric binding site, chemical structure, and the predicted binding mode of compound Z1078601926 in hDAT. (A) Allosteric binding site on hDAT used for virtual screening. (B) Chemical structure of Z1078601926. (C) Docking pose of Z1078601926 (orange, stick) in the allosteric site. The polar interactions with residues (blue, line) of Glu117 and Glu490 in the site are shown in red dashed lines.

inhibitor of hDAT. The molecular mechanism underlying the allosteric inhibition of hDAT by Z1078601926 was also elucidated using MD simulation.

## RESULTS AND DISCUSSION

The IO conformation is an essential state for hDAT to reuptake DA from the synaptic cleft into presynaptic neurons.<sup>21</sup> Currently, no structure of hDAT in the IO state or inhibitors targeting the conformation has been reported. Here, the structure-based strategy (Figure 1) was proposed to identify novel allosteric inhibitors against hDAT in IO conformation.

**Intermediate Stable State of hDAT (IO) Revealed by GaMD.** The initial structure of hDAT in IO conformation was first constructed by MODELLER,<sup>22</sup> where the Cryo-EM structure of hSERT in the same conformation (PDB ID: 6DZZ<sup>9</sup>) was chosen as the template. The structure with the best performance in protein geometry was selected as the model of hDAT (Table S3). Then, Na<sup>+</sup> and Cl<sup>-</sup> ions were fitted into the corresponding binding sites of hDAT and with DA docked into the S1 site through an induced fit method.<sup>23</sup> To explore the intermediate stable state of hDAT in IO conformation, 2  $\mu$ s of all-atom GaMD simulation in an explicit membrane environment was implemented, which boosted both the dihedral and total potential energy of the system to increase the flexibility of conformational shifting in the simulation.<sup>24</sup> Finally, two-dimensional PMF was calculated to illustrate the free energy landscape of the system, of which the regarded distance of residue/ligand pairs was set as Phe76–Asp79 and Asp79–DA (Figure 2). These two residues at TM1 of hDAT relate to the substrate binding of the S1 site and the conformational change from OO to IO. The DA binding to the orthosteric site was confined in two energy wells (Figure 2A), which were centered at (6.0, 9.1 Å) and (6.3, 4.7 Å), respectively. This suggests that equilibrium states of S1 site substrate binding exist in potentially two substates (Figures 2 and S1). The structure cluster of the well at (6.0, 9.1 Å) was

determined by the near-native conformation (Figure 2B) and extracted for further allosteric study.

**Allosteric Site Prediction and Virtual Screening.** The potential allosteric sites on the energetic stable IO state of hDAT were detected by SiteMap.<sup>25</sup> The properties of the top five druggable sites are listed in Table S1 and their locations are shown in Figure S2. Four sites these sites were located in the intracellular region and one site was situated in the extracellular region. All of the predicted sites performed with both SiteScore and Dscore above 0.9 and diversity in hydrophobicity and hydrophilicity (Table S1). To investigate the potential drug binding to hDAT in IO conformation, the overall best-scoring intracellular site (Figure 3A) was used for defining the docking grid box. Also, ~440,000 compounds from seven enamine libraries were subjected to Glide virtual screening workflow (VSW). Twenty-five top-ranking compounds with better binding modes and docking scores were selected for hierarchical clustering analysis based on 2D fingerprints.<sup>26</sup> As a result, 10 compounds with diverse scaffolds (Table S2) were purchased for further *in vitro* assay.

Using Z1078601926 (Figure 3B) with allosteric inhibition activity (see “*In Vitro Assay of Allosteric Inhibition*” section below) as an example, the docking result showed that the compound binds to the pocket formed by residues Glu117, Lys133, Lys139, Val141, Gly142, Val145, Gly325, Ile330, Thr431, Gly432, Asp435, Glu436, and Phe437, where key interactions occurred between the nitrogen in the pyrrolidine ring of Z1078601926 and both of the oxygens in carboxylic acid of Glu117 and Glu436 (Figure 3C).

***In Vitro Assay of Allosteric Inhibition.*** In this study, dose–response dopamine reuptake inhibition assay was realized by the reagent of Neurotransmitter Transporter Uptake Assay Kit, which mimics DA and acts as a fluorescent indicator.<sup>27,28</sup> Stably transfected HEK293T cells expressing hDAT confirmed by quantitative real-time polymerase chain reaction (PCR) were used for the assay (Figure S3).

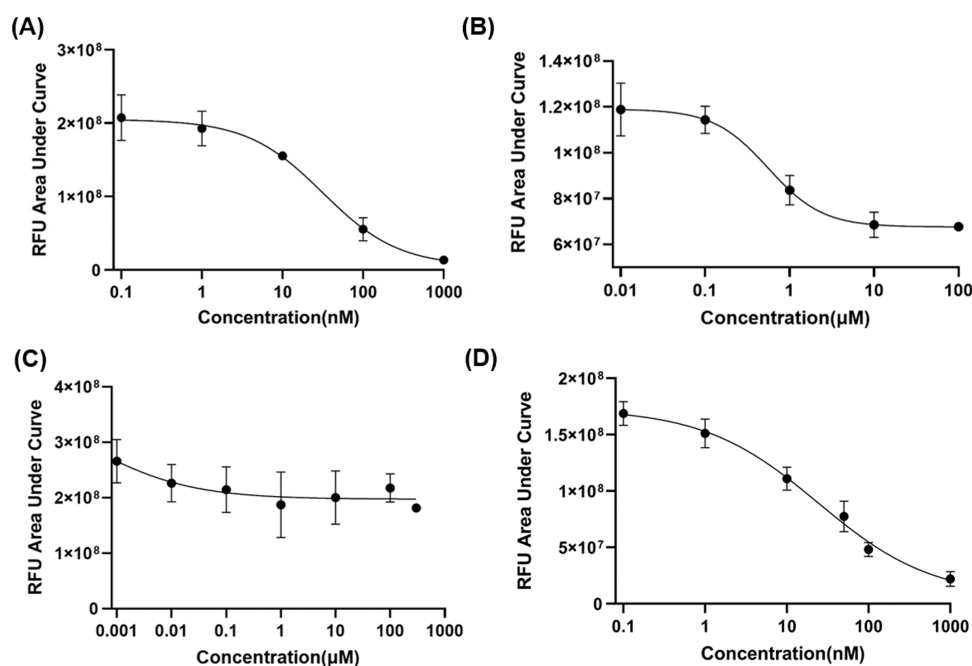


**Figure 4.** Inhibition assay by neurotransmitter transporter uptake assay kit. (A) Inhibition assay of nomifensine. Monoamines reuptake volume was depicted as the area under the curve of relative fluorescence unit (RFU). (B) Thirty-one nanomolar nomifensine was previously added for the allosteric inhibition assay of Z1078601926 in hDAT. (C) Inhibition assay with Z1078601926 introduced previously presented no obvious orthosteric inhibition on hDAT implied by the slight RFU reduction. (D) Z1078601926 (0.527  $\mu\text{M}$ ) was previously added for the orthosteric inhibition assay of nomifensine in hDAT.

**Table 1.** Estimated MM/GBSA Binding Free Energies ( $\Delta G_{\text{MM/GBSA}}$ , kcal mol<sup>-1</sup>) and Inhibition Activity ( $\text{IC}_{50}$ ) of Z1078601926 and Nomifensine to hDAT

system	$\Delta E_{\text{ele}}^a$	$\Delta E_{\text{vdW}}^b$	$\Delta G_{\text{pol}}^c$	$\Delta G_{\text{nonpol}}^d$	$\Delta G_{\text{MM/GBSA}}^e$	$\text{IC}_{50}^f$
Z1078601926-hDAT	-146.46	-29.66	155.24	-3.29	$-24.18 \pm 4.21$	<sup>g</sup>
Z1078601926-hDAT (nomifensine bound)	-112.31	-35.91	125.67	-3.33	$-25.88 \pm 3.12$	0.527 [0.284; 0.988] <sup>h</sup> $\mu\text{M}$
nomifensine-hDAT	-62.06	-33.25	67.27	-3.04	$-31.08 \pm 2.69$	31.01 [15.50; 104.9] nM
nomifensine-hDAT (Z1078601926 bound)	-50.98	-34.64	56.48	-3.02	$-32.16 \pm 2.36$	24.21 [11.67; 99.10] nM

<sup>a</sup>The electrostatic interaction energy ( $\Delta E_{\text{ele}}$ ) in the gas phase. <sup>b</sup>The van der Waals interaction energy ( $\Delta E_{\text{vdW}}$ ) in the gas phase. <sup>c</sup>The free energy of polar solvation ( $\Delta G_{\text{pol}}$ ). <sup>d</sup>The free energy of nonpolar solvation ( $\Delta G_{\text{nonpol}}$ ). <sup>e</sup>The total binding free energy,  $\Delta G_{\text{MM/GBSA}} = \Delta E_{\text{ele}} + \Delta E_{\text{vdW}} + \Delta G_{\text{pol}} + \Delta G_{\text{nonpol}}$ . <sup>f</sup>The inhibition activity against dopamine reuptake and the concentration-gradient assay resulted in about 50% of maximum uptake inhibition by the reduction of relative fluorescence unit (RFU). <sup>g</sup>The compound resulted in a slight RFU reduction and no obvious inhibition activity. <sup>h</sup>The assay was repeated three times and the 95% confidence interval standard deviation of  $\text{IC}_{50}$ .

First, to examine the reuptake efficiency of hDAT with ligand bound, the dopamine reuptake inhibitor (DRI) nomifensine that selectively binds at the orthosteric site was introduced into the assay, resulting in the maximum uptake inhibition of 95% and  $\text{IC}_{50}$  of 31.01 [15.50; 104.9] nM demonstrated by the relative fluorescence intensity (Figure 4A), which is similar to the literature record and validated the method.<sup>29</sup>

Then, to test the allosteric modulation of 10 purchased compounds at a concentration of 10 nM, the orthosteric ligand nomifensine was introduced into the assay with a concentration of its  $\text{IC}_{50}$ , which refers to a certain orthosteric inhibition and helps to identify whether the ligand present positively or negatively in allosteric modulation.<sup>30</sup> Among the tested compounds, Z1078601926 displayed a further inhibition against dopamine reuptake, and the concentration-gradient assay resulted in about 50% of maximum uptake inhibition by the reduction of relative fluorescence unit (RFU) ( $\text{IC}_{50} = 0.527$  [0.284; 0.988]  $\mu\text{M}$ , Figure 4B). Meanwhile, the result suggests that Z1078601926 partially enhanced the inhibition against hDAT, reaching a total uptake inhibition of 75%, with

50% of background inhibition contributed by nomifensine revealed by the starting point of the assay compared with the assay of nomifensine solely. In addition, an assay with a concentration gradient of Z1078601926 without nomifensine revealed that the compound resulted in a slight RFU reduction and had no obvious inhibition activity (Figure 4C), which implies the synergistic effect between Z1078601926 and nomifensine that selectively binds to the allosteric and orthosteric sites of hDAT, respectively.

Finally, a reverse dose–response assay of nomifensine with Z1078601926 presented in  $\text{IC}_{50}$  concentration was implemented, where the decreased value of the  $\text{IC}_{50}$  (24.21 [11.67; 99.10] nM) from the RFU data suggests that the presence of Z1078601926 enhances the inhibition efficacy nomifensine, which further demonstrates their synergistic inhibition effect on hDAT (Figure 4D).

These results suggest that the synergistic effect between nomifensine and Z1078601926 enhances their inhibition efficiency against hDAT to a certain degree. Meanwhile, the inhibition of Z1078601926 to hDAT is not as significant as that of nomifensine. Nevertheless, the two compounds worked

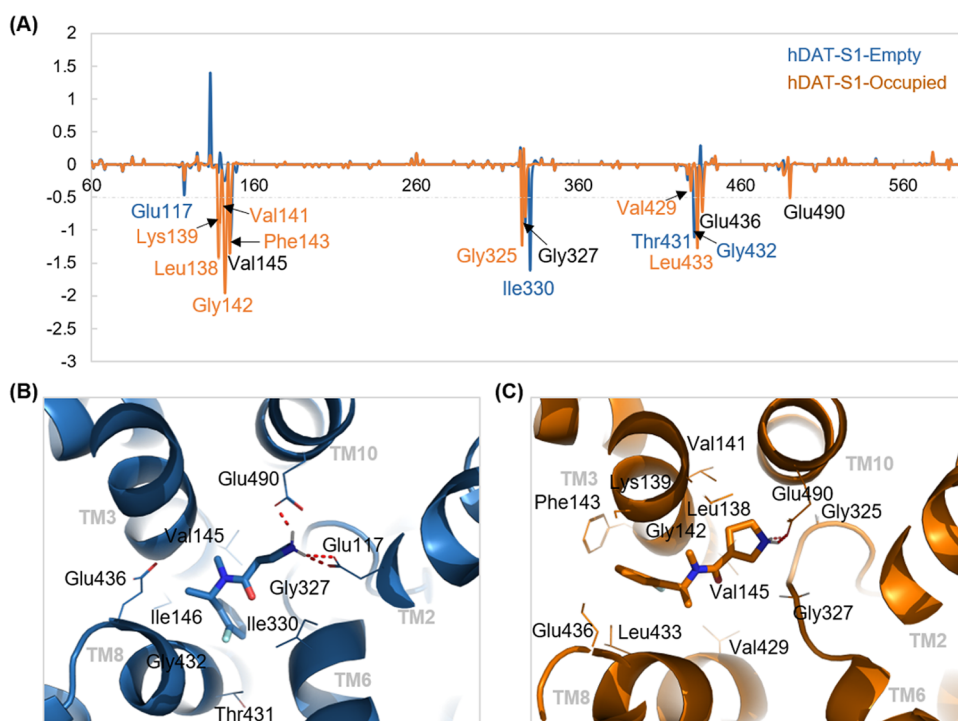


**Figure 5.** Structure and energy profiles of Z1078601926 bound to the allosteric site of hDAT with or without nomifensine located at the orthosteric site. (A) Energies of residues in hDAT contribute to the binding of Z1078601926. (B, C) Binding mode between hDAT and Z1078601926. hDAT and Z1078601926 are displayed as cartoon and stick representations, respectively. Only the important residues (the absolute energy contribution  $\geq 0.5$  kcal mol $^{-1}$ ) were labeled. The hydrogen bond is shown in the red dashed line.

as an allostery pattern targeting hDAT in an inward-open conformation, which could be regarded as a good starting point for further research studies on the allosteric modulator of hDAT.

**Mechanism of the Allosteric Inhibition of hDAT by Z1078601926.** To understand the molecular mechanism underlying the allosteric inhibition of hDAT by Z1078601926 when nomifensine was introduced, three additional simulation systems (hDAT complexed with Z1078601926 and nomifensine simultaneously, hDAT complexed with only Z1078601926 or nomifensine) were designed and submitted for 1  $\mu$ s GaMD run. Based on the MD trajectories, the estimated binding free energies ( $\Delta G_{\text{calc}}$ ) of Z1078601926 to hDAT with or without nomifensine existing at the orthosteric site were  $-24.18$  and  $-25.88$  kcal mol $^{-1}$  (Table 1), respectively. The  $\Delta G_{\text{calc}}$  indicated that Z1078601926 had a higher affinity to hDAT when nomifensine occupied the orthosteric site, which was consistent with the experimental inhibition activities. Meanwhile, the  $\Delta G_{\text{calc}}$  of nomifensine to hDAT was  $-31.08$  kcal mol $^{-1}$ , which had a relatively low binding affinity to hDAT compared with that of nomifensine bound to hDAT when Z1078601926 presented ( $-32.16$  kcal mol $^{-1}$ ), which demonstrated the effects of the newly discovered allosteric inhibitor.

In addition, the important residues (the absolute energy contribution  $\geq 0.5$  kcal mol $^{-1}$ ) located at the allosteric site of hDAT contributing to the Z1078601926 binding in both systems were identified through per-residue energy decomposition analysis (Figure 5A). The distribution of the important residues indicated that Z1078601926 had a similar binding mechanism to the allosteric site of hDAT in the two simulation systems (Figure 5A), which shared four common residues (Val145, Gly327, Glu436, and Glu490). To verify the

binding mode of the compound, *in silico* alanine scanning of Val145Ala, Glu436Ala, and Glu490Ala was conducted. As a result, the calculated binding free energy difference ( $\Delta\Delta G_{\text{calc}} = \Delta G_{\text{mut}} - \Delta G_{\text{wt}}$ ) between the mutant (mut) and wild-type (wt) complexes were 1.16, 0.96, and 4.53 kcal mol $^{-1}$  for Val145Ala, Glu436Ala, and Glu490Ala complexes, respectively, demonstrating that those residues play an essential role in recognition and binding of Z1078601926 to hDAT. It was noted that *in silico* alanine scanning of Gly327 was not carried out herein; this is because the size of Gly is the smallest among the 20 natural amino acids, and the method only works on the mutation of residues with a size larger than that of alanine.<sup>31</sup>

Moreover, the binding modes of Z1078601926 in hDAT with or without nomifensine bound are shown in Figure 5B,C, respectively, and with the identified important residues mapped on the pocket. Compared to hDAT in complex with Z1078601926 alone (Figure 5B), nomifensine binding at the orthosteric site induced the conformational change of Z1078601926 at the allosteric site (Figure 5C), leading to the pocket reshaping, which is clearly demonstrated by the unique residues identified in each complex (Figure 5A). Therefore, it is proposed that the synergistic effect between Z1078601926 and nomifensine is the major mechanism of the observed allosteric inhibition of hDAT by Z1078601926, which should be further validated by experimental analysis such as structural biology study.

## CONCLUSIONS

In this study, the intermediate stable state of hDAT presented in the IO conformation was first characterized by GaMD simulation and free energy landscape analysis. Then, a druggable allosteric site was identified in the intracellular region of the transporter and used for virtual screening. Further

*in vitro* assay identified Z1078601926, one of the test compounds showed allosteric inhibition of hDAT ( $IC_{50} = 0.527 [0.284; 0.988] \mu\text{M}$ ) when nomifensine was introduced as an orthosteric ligand. In addition, a synergistic effect for the allosteric inhibition of hDAT by Z1078601926 and nomifensine was explored by GaMD simulations of two designed systems postbinding free energies analysis, which could be further investigated. Moreover, the predicted model of Z1078601926 in complex with hDAT and identified the key residues (Val145, Gly327, Glu436, and Glu490) contribute to the fact that compound binding could provide an important starting point for allosteric lead compound optimization.

## MATERIALS AND METHODS

**System Preparation. Homology Modeling.** Since no crystal structure of hDAT has been resolved so far, homology modeling was utilized to generate the structural model of inward-open (IO) hDAT, of which the template was derived from the Cryo-EM structure of hSERT (PDB ID: 6DZZ).<sup>9</sup> The hSERT structure was modified by the Protein Preparation Wizard tool in Schrödinger.<sup>32</sup> The alignment of hDAT (Uniprot entry: Q01959) and hSERT amino acid sequences was implemented by UCSF Chimera,<sup>33</sup> and homology models of hDAT were built by MODELLER.<sup>22</sup> The 5 high-scoring models were evaluated by MolProbity,<sup>34</sup> and the best one performing in protein geometry was selected. Moreover, the functional  $\text{Na}^+/\text{Cl}^-$  pair in IO hDAT was manually fit into the ion-binding sites of hDAT through the align module in PyMOL.

**Orthosteric Ligand Docking.** The 3D structure of dopamine was obtained from PubChem (PubChem CID: 681), and LigPrep with the OPLS3 force field was utilized to minimize the DA structure. In addition, the ionized state of DA was realized by Epik at a pH value of  $7.0 \pm 2.0$  for docking.<sup>35</sup>

Glide-induced fit docking (IFD) was processed to dock DA into the S1 site. The centroid was defined by the residues related to the S1 site binding recorded by previous studies with the OPLS3 force field.<sup>36</sup> The reasonable pose of DA binding was selected, compared with the orientation of escitalopram in the hSERT structure.<sup>37</sup>

**Construction of Protein–Ligand/Membrane Systems.** The prepared complex structure was pre-oriented in OPM<sup>38</sup> and inserted into an explicit POPC lipid bilayer with  $\sim 185$  lipids by means of a membrane builder module in CHARMM-GUI.<sup>39</sup> The TIP3P water of 40 Å thickness was placed above and below the constructed bilayer, and the  $\text{Na}^+$  and  $\text{Cl}^-$  counterions were used to neutralize the systems at an environmental salt concentration of 0.15 M, resulting in the whole system forming a periodic cell ( $90 \text{ \AA} \times 90 \text{ \AA} \times 120 \text{ \AA}$ ) containing  $\sim 83,000$  atoms.

**Force Field Parameters.** LEaP was used to assign force field parameters for each partner of the complex, and the hDAT protein, POPC lipids,  $\text{Na}^+$  and  $\text{Cl}^-$  ions, and TIP3P waters were described using AMBER ff14SB,<sup>40</sup> Lipid14,<sup>41</sup> and monovalent ion parameters for TIP3P water, respectively. AMBER force field 2 (GAFF2) parameter<sup>42</sup> sets for the ligands (DA, nomifensine, and Z1078601926) and the partial charges were derived from RESP calculation using an HF/6-31G\* electrostatic potential calculated by Gaussian09.

**Molecular Dynamics Simulations.** In this work, four systems (DA-hDAT, nomifensine-hDAT, Z1078601926-hDAT, and nomifensine-Z1078601926-hDAT) were prepared

and subjected to MD simulations with a GPU-accelerated version of AMBER18.

**Conventional Molecular Dynamics Simulation.** To eliminate bad contacts between the solute and solvent water molecules in the system, energy minimization and equilibration simulations were accomplished in three sections before production simulation. First, energy minimization was adopted to apply a harmonic restraint on the lipid and the solute atom (force constant =  $10 \text{ kcal mol}^{-1} \text{ \AA}^{-2}$ ), and then the entire system was minimized for 10,000 steps followed by energy minimization of 5000 steps using the Steepest Descent algorithm and the conjugate gradient method. Second, a two-step equilibration was performed, each system was heated from 0 K to approximately 100 K and then gradually to 310 K with the protein and lipid restrained over 100 ps in the NVT ensembles. Then, all the simulated complexes were repeated for 10 times unconstrained NPT dynamics (5 ns) at 310 K and 1 atm. Finally, a 100 ns MD production simulation was performed for each complex with a durations in the NPT ensemble at 310 K and 1 atm using the periodic boundary condition, where the temperature and pressure were maintained using a Langevin thermostat and a Monte Carlo barostat, respectively. Electrostatic interactions with a distance cutoff of 10 Å were calculated using the Particle-Mesh Ewald (PME) method. The SHAKE algorithm was used to keep all-bonds constraints, and the time step was set as 2.0 fs.<sup>43</sup>

**Gaussian-Accelerated Molecular Dynamics Simulation.** GaMD is a biomolecular enhanced sampling method that works by adding a harmonic boost potential to smoothen the system potential energy surface. The boost potential introduced into the system follows a Gaussian distribution, which allows for accurate reweighting using cumulant expansion of the second order.

The basic detailed theory of GaMD was described in a previously published study.<sup>24</sup> Briefly, for a system with  $N$  atoms at positions  $\vec{\gamma} = \{\vec{\gamma}_1, \dots, \vec{\gamma}_N\}$ , the system energy  $V(\gamma)$  is modified by adding a potential  $\Delta V$  whenever it is below a threshold energy  $E$ , which is defined as

$$V^*(\gamma) = V(\gamma) + \Delta V \quad (1)$$

$$\Delta V = \begin{cases} \frac{1}{2}k(E - V(r)), & V(r) < E \\ 0, & V(r) \geq E \end{cases} \quad (2)$$

where  $k$  is the harmonic force constant, and in this simulation, two adjustable parameters were set as  $k = 1$  and  $E = V_{\text{max}}$ .

For each system, the initial structure of the whole GaMD simulation was derived from the ultimate structure of cMD simulation, and relative long continuous GaMD simulations were performed for DA-hDAT, nomifensine-hDAT, Z1078601926-hDAT, and nomifensine-Z1078601926-hDAT, where both dihedral and total potential energy was boosted.

All MD simulations were performed on a GPU-accelerated version of AMBER18.

**Free Energy Landscape Analysis and Structure Clustering.** CPPTRAJ<sup>44</sup> was used to analyze the trajectories of GaMD simulations, where distances between the precise atoms in residue pairs were calculated, including the  $C_\beta$  of Phe76-the  $C_\gamma$  of Asp79 and the  $C_\gamma$  of Asp79-the  $N_1$  of DA. PyReweighting<sup>45</sup> provides algorithms of exponential average, Maclaurin series, and cumulant expansion for reweighting the GaMD simulation, and cumulant expansion was chosen for the

energetic reweighting of the energy landscape, where the boosted energy was sampled every 5000 steps. Two-dimensional PMF profiles regarding the distances of two atom pairs were drawn, with the cutoff set to 10 frames. The clustering of trajectory frames was realized by CPPTRAJ implemented with the DBSCAN algorithm.

**Allosteric Site Prediction.** SiteMap was utilized to predict the potential allosteric pocket on hDAT in IO conformation, which operates in a manner similar to Goodford's GRID algorithm but employs a unique definition of hydrophobicity.<sup>25</sup> The representative hDAT protein–ligand structure was prepared by the Protein Preparation Wizard tool in Schrödinger.<sup>32</sup> The total process of SiteMap was run in three stages. First, relevant site points are selected based on geometric and energetic properties, and the points are grouped into sets to define the sites. Second, hydrophobic, hydrophilic, and other key properties are computed at grid points and contour maps are prepared. Finally, site properties such as SiteScore and Dscore are computed. The site searching region was set in whole protein, and the minimum grid number was constrained to 15 with stricter hydrophobic and hydrophilic assays.<sup>46</sup>

**Virtual Screening and Cheminformatic Analysis.** Seven enamine chemical libraries containing ~440,000 molecules were selected for Glide virtual screening,<sup>47</sup> where all of the compounds were prepared by the LigPrep program, and all compounds were processed through generating tautomers, stereoisomers, and ionization states by Epik<sup>35</sup> under the condition of  $7.0 \pm 2.0$  pH value with the OPLS3 force field.<sup>48</sup>

Screening of the libraries was processed via docking into the grid of the site defined by SiteMap, undergoing HTVS, SP, and XP segments, where 10% of the top-scoring molecules were maintained. The result sets were further filtered by the Prime MM-GBSA method. The top-ranking molecules were clustered by chemical similarity in Canvas.<sup>49</sup>

**MM/GBSA Binding Free Energy.** The molecular mechanics/generalized born surface area (MM/GBSA) method was utilized to calculate the binding free energy ( $\Delta G_{\text{calc}}$ ) of Z1078601926 and nomifensine to hDAT.<sup>50–55</sup> The calculation followed the equation below

$$\Delta G_{\text{calc}} = \Delta E_{\text{vdW}} + \Delta E_{\text{ele}} + \Delta G_{\text{pol}} + \Delta G_{\text{nonpol}} \quad (3)$$

For each term,  $\Delta E_{\text{vdW}}$  refers to the van der Waals energies and  $\Delta E_{\text{ele}}$  refers to the electrostatic interaction energies in the gas phase.  $\Delta G_{\text{pol}}$  and  $\Delta G_{\text{nonpol}}$  represent the polar and nonpolar solvation energies, respectively.

**In Silico Alanine Scanning.** *In silico* alanine scanning study includes two steps. First, mutated snapshots were generated based on the simulation trajectory by truncating the selected mutation residue at C $\gamma$  and by replacing C $\gamma$  with a hydrogen atom.<sup>31</sup> Then, the binding free energy difference ( $\Delta\Delta G_{\text{calc}} = \Delta G_{\text{mut}} - \Delta G_{\text{wt}}$ ) between the wild-type (wt) and mutant (mut) complexes is calculated.  $\Delta G_{\text{mut}}$  and  $\Delta G_{\text{wt}}$  refer to the MM/GBSA binding free energy of the mut and wt complexes, respectively.

**Cell Culture and Transfection.** HEK293T cells were maintained in DMEM (4.5 g L<sup>-1</sup> glucose), supplemented with 10% fetal bovine serum (FBS) at 37 °C with 5% CO<sub>2</sub>. Vectors containing mRNA of hDAT (NCBI ID: NM\_001044.5) CDS fragment in plasmid were transfected into the cell by Attractane Transfection Reagent (Qiagen, Hilden, Germany),

introduced with 2  $\mu\text{g mL}^{-1}$  puromycin to maintain the expression.

**Quantitative Real-Time PCR.** Quantitative real-time PCR was utilized to confirm the high expression of hDAT in the transfected cell lines. Total RNA was isolated using RNA Easy Fast Cell Kit (Tiangen Biotech, Beijing, China), and cDNA synthesis was processed by OneStep RT-PCR Kit (Qiagen, Hilden, Germany). Quantitative PCR was performed by LightCycler 480 system (Roche, Basel, Switzerland), with the reagent of TB Green Premix EX Taq II (TaKaRa Bio Inc, Shiga, Japan). The amplification of target cDNA was normalized to GAPDH expression. Relative levels of target mRNA expression were calculated using the standard curve method. The sequences of primer pairs are described below:

hDAT:

5' GTCTGTTTGGATTGACGCGG 3' (forward)

3' GTGACAATCGCGTCCCTGTA 5' (reverse)

GAPDH:

5' TGTGGGCATCAATGGATTTGG 3' (forward)

3' ACACCATGTATTCCGGGTCAAT 5' (reverse)

**Transport Inhibition Assays.** The compound of nomifensine and Z1078601926 were purchased from Topscience, Shanghai. All of the reuptake inhibitory activity against DA was measured by Neurotransmitter Transporter Uptake Assay Kit (Molecular Devices, Sunnyvale, California), which contains a novel proprietary fluorescent indicator dye that mimics dopamine and is actively transported into the cells via the dopamine transporters, resulting in increased intracellular fluorescence intensity, which refers to the efficiency of dopamine reuptake.<sup>27</sup> The transfected cells were incubated in the respective concentration of compounds dissolved in HBSS-0.1% BSA buffer in a 96-well plate for 30 min. After that, a dye solution was introduced and immediately the fluorescence intensity was kinetically read by SpectraMax i3x (Molecular Devices, Sunnyvale, California) for 30 min. By removing the background fluorescence of the solution in an assay, raw data of detected RFU was reduced by the mean of area under the curve in SoftMax Pro 7 and IC<sub>50</sub> (mean, [95% confidence interval of standard deviation,  $n = 3$ ]) was calculated by four-logistic parameter fit in GraphPad Prism 9. All of the assays were implemented with three replicates.

## ■ ASSOCIATED CONTENT

### Data Availability Statement

The input files, parameter files, topology files, and trajectory analysis scripts used to generate the results in this work, as well as the representative structure of each simulation are provided as the Supporting Information. The MD trajectory in this work is available in Zenodo at <https://doi.org/10.5281/zenodo.7750922>.

### Supporting Information

The Supporting Information is available free of charge at <https://pubs.acs.org/doi/10.1021/acs.jcim.3c00477>.

Information of the five top-ranking allosteric sites predicted by SiteMap; geometry statistics of the best-performing hDAT homology model by MolProbity; structure and free energy landscape of DA in complex with IO' hDAT; quantitative real-time PCR analysis of hDAT (hSLC6A3) expression; additional experimental details and results of the study, including the data set of simulation and analysis (PDF)

Data S1 (ZIP)

## AUTHOR INFORMATION

### Corresponding Authors

**Haiwei Zhang** – Chongqing Key Laboratory of Translational Research for Cancer Metastasis and Individualized Treatment, Department of Pathology, Chongqing University Cancer Hospital, Chongqing 400030, China; Email: [haiweizh@cqu.edu.cn](mailto:haiweizh@cqu.edu.cn)

**Weiwei Xue** – Chongqing Key Laboratory of Natural Product Synthesis and Drug Research, School of Pharmaceutical Sciences, Chongqing University, Chongqing 401331, China; [orcid.org/0000-0002-3285-0574](https://orcid.org/0000-0002-3285-0574); Email: [xueww@cqu.edu.cn](mailto:xueww@cqu.edu.cn)

### Authors

**Shengzhe Deng** – Chongqing Key Laboratory of Natural Product Synthesis and Drug Research, School of Pharmaceutical Sciences, Chongqing University, Chongqing 401331, China

**Rongpei Gou** – Chongqing Key Laboratory of Natural Product Synthesis and Drug Research, School of Pharmaceutical Sciences, Chongqing University, Chongqing 401331, China

**Ding Luo** – Chongqing Key Laboratory of Natural Product Synthesis and Drug Research, School of Pharmaceutical Sciences, Chongqing University, Chongqing 401331, China; [orcid.org/0009-0000-9326-319X](https://orcid.org/0009-0000-9326-319X)

**Zerong Liu** – Central Nervous System Drug Key Laboratory of Sichuan Province, Sichuan Credit Pharmaceutical Co., Ltd., Luzhou 646000, China; [orcid.org/0000-0003-4343-7643](https://orcid.org/0000-0003-4343-7643)

**Feng Zhu** – College of Pharmaceutical Sciences, Zhejiang University, Hangzhou 310058 Zhejiang, China; [orcid.org/0000-0001-8069-0053](https://orcid.org/0000-0001-8069-0053)

Complete contact information is available at: <https://pubs.acs.org/10.1021/acs.jcim.3c00477>

### Author Contributions

W.X., H.Z., and S.D. designed the research. S.D., H.Z., R.G., and D.L. performed the research. S.D., Z.L., F.Z., and W.X. analyzed the data. S.D. and W.X. wrote the manuscript. All authors reviewed the manuscript.

### Notes

The authors declare no competing financial interest.

## ACKNOWLEDGMENTS

The authors thank Prof. Xiaojun Yao at Lanzhou University for help and discussion on induced fit docking. This work was supported by the Natural Science Foundation of China (21505009), the Open Project of Central Nervous System Drug Key Laboratory of Sichuan Province (230012-01SZ), and the Entrepreneurship and Innovation Support Plan for Chinese Overseas Students of Chongqing (cx2020127).

## ABBREVIATIONS

hDAT, human dopamine transporter; DA, dopamine; SLC6, solute carrier 6; NSS, neurotransmitter sodium symporter; ADHD, attention deficit hyperactivity disorder; PD, Parkinson's disease; CNS, central nervous system; LeuT, leucine transporter; dDAT, *Drosophila melanogaster* dopamine transporter; hSERT, human serotonin transporter; TM, transmembrane domain; IL, intracellular loop; EL, extracellular loop; OO, outward-open; OC, occluded; IO, inward-open;

DRI, dopamine reuptake inhibitor; RFU, relative fluorescence unit; GaMD, Gaussian-accelerated molecular dynamics; PMF, potentials of mean force; Cryo-EM, Cryo-electron microscopy; MM/GBSA, molecular mechanics generalized born surface area

## REFERENCES

- (1) Masson, J.; Sagne, C.; Hamon, M.; El Mestikawy, S. Neurotransmitter transporters in the central nervous system. *Pharmacol. Rev.* **1999**, *51*, 439–464.
- (2) Chen, N.; Reith, M. E. Structure and function of the dopamine transporter. *Eur. J. Pharmacol.* **2000**, *405*, 329–339.
- (3) Vaughan, R. A.; Foster, J. D. Mechanisms of dopamine transporter regulation in normal and disease states. *Trends Pharmacol. Sci.* **2013**, *34*, 489–496.
- (4) Pramod, A. B.; Foster, J.; Carvelli, L.; Henry, L. K. SLC6 transporters: structure, function, regulation, disease association and therapeutics. *Mol. Aspects Med.* **2013**, *34*, 197–219.
- (5) Mackie, P.; Lebowitz, J.; Saadatpour, L.; Nickoloff, E.; Gaskill, P.; Khoshbouei, H. The dopamine transporter: An unrecognized nexus for dysfunctional peripheral immunity and signaling in Parkinson's Disease. *Brain, Behav., Immun.* **2018**, *70*, 21–35.
- (6) Zhou, Y.; Zhang, Y.; Lian, X.; Li, F.; Wang, C.; Zhu, F.; Qiu, Y.; Chen, Y. Therapeutic target database update 2022: facilitating drug discovery with enriched comparative data of targeted agents. *Nucleic Acids Res.* **2022**, *50*, D1398–D1407.
- (7) Yamashita, A.; Singh, S. K.; Kawate, T.; Jin, Y.; Gouaux, E. Crystal structure of a bacterial homologue of Na<sup>+</sup>/Cl<sup>-</sup>-dependent neurotransmitter transporters. *Nature* **2005**, *437*, 215–223.
- (8) Penmatsa, A.; Wang, K. H.; Gouaux, E. X-ray structure of dopamine transporter elucidates antidepressant mechanism. *Nature* **2013**, *503*, 85–90.
- (9) Coleman, J. A.; Yang, D.; Zhao, Z.; Wen, P. C.; Yoshioka, C.; Tajkhorshid, E.; Gouaux, E. Serotonin transporter-ibogaine complexes illuminate mechanisms of inhibition and transport. *Nature* **2019**, *569*, 141–145.
- (10) Cheng, M. H.; Bahar, I. Monoamine transporters: structure, intrinsic dynamics and allosteric regulation. *Nat. Struct. Mol. Biol.* **2019**, *26*, 545–556.
- (11) Hasenhuettl, P. S.; Bhat, S.; Freissmuth, M.; Sandtner, W. Functional Selectivity and Partial Efficacy at the Monoamine Transporters: A Unified Model of Allosteric Modulation and Amphetamine-Induced Substrate Release. *Mol. Pharmacol.* **2019**, *95*, 303–312.
- (12) Xue, W.; Fu, T.; Zheng, G.; Tu, G.; Zhang, Y.; Yang, F.; Tao, L.; Yao, L.; Zhu, F. Recent Advances and Challenges of the Drugs Acting on Monoamine Transporters. *Curr. Med. Chem.* **2020**, *27*, 3830–3876.
- (13) Aggarwal, S.; Mortensen, O. V. Overview of Monoamine Transporters. *Curr. Protoc. Pharmacol.* **2017**, *79*, 12–16.
- (14) Rothman, R. B.; Dersch, C. M.; Ananthan, S.; Partilla, J. S. Studies of the biogenic amine transporters. 13. Identification of "agonist" and "antagonist" allosteric modulators of amphetamine-induced dopamine release. *J. Pharmacol. Exp. Ther.* **2009**, *329*, 718–728.
- (15) Aggarwal, S.; Liu, X.; Rice, C.; Menell, P.; Clark, P. J.; Paparoidamis, N.; Xiao, Y. C.; Salvino, J. M.; Fontana, A. C. K.; Espana, R. A.; Kortagere, S.; Mortensen, O. V. Identification of a Novel Allosteric Modulator of the Human Dopamine Transporter. *ACS Chem. Neurosci.* **2019**, *10*, 3718–3730.
- (16) Piscitelli, C. L.; Krishnamurthy, H.; Gouaux, E. Neurotransmitter/sodium symporter orthologue LeuT has a single high-affinity substrate site. *Nature* **2010**, *468*, 1129–1132.
- (17) Kortagere, S.; Fontana, A. C.; Rose, D. R.; Mortensen, O. V. Identification of an allosteric modulator of the serotonin transporter with novel mechanism of action. *Neuropharmacology* **2013**, *72*, 282–290.

- (18) Tu, G.; Xu, B.; Luo, D.; Liu, J.; Liu, Z.; Chen, G.; Xue, W. Multi-state Model-Based Identification of Cryptic Allosteric Sites on Human Serotonin Transporter. *ACS Chem. Neurosci.* **2023**, *14*, 1686–1694.
- (19) Xue, W.; Fu, T.; Deng, S.; Yang, F.; Yang, J.; Zhu, F. Molecular Mechanism for the Allosteric Inhibition of the Human Serotonin Transporter by Antidepressant Escitalopram. *ACS Chem. Neurosci.* **2022**, *13*, 340–351.
- (20) Niello, M.; Gradisch, R.; Loland, C. J.; Stockner, T.; Sitte, H. H. Allosteric Modulation of Neurotransmitter Transporters as a Therapeutic Strategy. *Trends Pharmacol. Sci.* **2020**, *41*, 446–463.
- (21) Nielsen, A. K.; Moller, I. R.; Wang, Y.; Rasmussen, S. G. F.; Lindorff-Larsen, K.; Rand, K. D.; Loland, C. J. Substrate-induced conformational dynamics of the dopamine transporter. *Nat. Commun.* **2019**, *10*, No. 2714.
- (22) Webb, B.; Sali, A. Comparative Protein Structure Modeling Using MODELLER. *Curr. Protoc. Bioinf.* **2016**, *54*, 5–6.
- (23) Sherman, W.; Day, T.; Jacobson, M. P.; Friesner, R. A.; Farid, R. Novel procedure for modeling ligand/receptor induced fit effects. *J. Med. Chem.* **2006**, *49*, 534–553.
- (24) Miao, Y.; Feher, V. A.; McCammon, J. A. Gaussian Accelerated Molecular Dynamics: Unconstrained Enhanced Sampling and Free Energy Calculation. *J. Chem. Theory Comput.* **2015**, *11*, 3584–3595.
- (25) Teixeira, O.; Lacerda, P.; Froes, T. Q.; Nonato, M. C.; Castilho, M. S. Druggable hot spots in trypanothione reductase: novel insights and opportunities for drug discovery revealed by DRUGpy. *J. Comput.-Aided Mol. Des.* **2021**, *35*, 871–882.
- (26) Sastry, M.; Lowrie, J. F.; Dixon, S. L.; Sherman, W. Large-scale systematic analysis of 2D fingerprint methods and parameters to improve virtual screening enrichments. *J. Chem. Inf. Model.* **2010**, *50*, 771–784.
- (27) Jørgensen, S.; Nielsen, E. O.; Peters, D.; Dyhring, T. Validation of a fluorescence-based high-throughput assay for the measurement of neurotransmitter transporter uptake activity. *J. Neurosci. Methods* **2008**, *169*, 168–176.
- (28) Molecular Devices. A Fluorescence Based Neurotransmitter Transporter Uptake Assay. <https://www.moleculardevices.com/sites/default/files/en/assets/scientific-posters/reagents/fluorescence-based-neurotransmitter-transporter-uptake-assay.pdf>.
- (29) Tatsumi, M.; Groshan, K.; Blakely, R. D.; Richelson, E. Pharmacological profile of antidepressants and related compounds at human monoamine transporters. *Eur. J. Pharmacol.* **1997**, *340*, 249–258.
- (30) Korczynska, M.; Clark, M. J.; Valant, C.; Xu, J.; Moo, E. V.; Albold, S.; Weiss, D. R.; Torosyan, H.; Huang, W.; Kruse, A. C.; Lyda, B. R.; May, L. T.; Baltos, J. A.; Sexton, P. M.; Kobilka, B. K.; Christopoulos, A.; Shoichet, B. K.; Sunahara, R. K. Structure-based discovery of selective positive allosteric modulators of antagonists for the M(2) muscarinic acetylcholine receptor. *Proc. Natl. Acad. Sci. U.S.A.* **2018**, *115*, E2419–E2428.
- (31) Huo, S.; Massova, I.; Kollman, P. A. Computational alanine scanning of the 1:1 human growth hormone-receptor complex. *J. Comput. Chem.* **2002**, *23*, 15–27.
- (32) Madhavi Sastry, G.; Adzhigirey, M.; Day, T.; Annabhimoju, R.; Sherman, W. Protein and ligand preparation: parameters, protocols, and influence on virtual screening enrichments. *J. Comput.-Aided Mol. Des.* **2013**, *27*, 221–234.
- (33) Pettersen, E. F.; Goddard, T. D.; Huang, C. C.; Couch, G. S.; Greenblatt, D. M.; Meng, E. C.; Ferrin, T. E. UCSF Chimera—a visualization system for exploratory research and analysis. *J. Comput. Chem.* **2004**, *25*, 1605–1612.
- (34) Chen, V. B.; Arendall, W. B., 3rd; Headd, J. J.; Keedy, D. A.; Immormino, R. M.; Kapral, G. J.; Murray, L. W.; Richardson, J. S.; Richardson, D. C. MolProbity: all-atom structure validation for macromolecular crystallography. *Acta Crystallogr., Sect. D: Biol. Crystallogr.* **2010**, *66*, 12–21.
- (35) Shelley, J. C.; Cholleti, A.; Frye, L. L.; Greenwood, J. R.; Timlin, M. R.; Uchimaya, M. Epik: a software program for pK(a) prediction and protonation state generation for drug-like molecules. *J. Comput.-Aided Mol. Des.* **2007**, *21*, 681–691.
- (36) Friesner, R. A.; Murphy, R. B.; Repasky, M. P.; Frye, L. L.; Greenwood, J. R.; Halgren, T. A.; Sanschagrin, P. C.; Mainz, D. T. Extra precision glide: docking and scoring incorporating a model of hydrophobic enclosure for protein-ligand complexes. *J. Med. Chem.* **2006**, *49*, 6177–6196.
- (37) Gabrielsen, M.; Ravna, A. W.; Kristiansen, K.; Sylte, I. Substrate binding and translocation of the serotonin transporter studied by docking and molecular dynamics simulations. *J. Mol. Model.* **2012**, *18*, 1073–1085.
- (38) Lomize, M. A.; Pogozheva, I. D.; Joo, H.; Mosberg, H. I.; Lomize, A. L. OPM database and PPM web server: resources for positioning of proteins in membranes. *Nucleic Acids Res.* **2012**, *40*, D370–D376.
- (39) Wu, E. L.; Cheng, X.; Jo, S.; Rui, H.; Song, K. C.; Davila-Contreras, E. M.; Qi, Y.; Lee, J.; Monje-Galvan, V.; Venable, R. M.; Klauda, J. B.; Im, W. CHARMM-GUI Membrane Builder toward realistic biological membrane simulations. *J. Comput. Chem.* **2014**, *35*, 1997–2004.
- (40) Maier, J. A.; Martinez, C.; Kasavajhala, K.; Wickstrom, L.; Hauser, K. E.; Simmerling, C. ffl4SB: Improving the Accuracy of Protein Side Chain and Backbone Parameters from ff99SB. *J. Chem. Theory Comput.* **2015**, *11*, 3696–3713.
- (41) Dickson, C. J.; Madej, B. D.; Skjevik, A. A.; Betz, R. M.; Teigen, K.; Gould, I. R.; Walker, R. C. Lipid14: The Amber Lipid Force Field. *J. Chem. Theory Comput.* **2014**, *10*, 865–879.
- (42) Wang, J.; Wolf, R. M.; Caldwell, J. W.; Kollman, P. A.; Case, D. A. Development and testing of a general amber force field. *J. Comput. Chem.* **2004**, *25*, 1157–1174.
- (43) Springborg, M.; Kirtman, B. Efficient vector potential method for calculating electronic and nuclear response of infinite periodic systems to finite electric fields. *J. Chem. Phys.* **2007**, *126*, No. 104107.
- (44) Roe, D. R.; Cheatham, T. E., 3rd. PTRAJ and CPPTRAJ: Software for Processing and Analysis of Molecular Dynamics Trajectory Data. *J. Chem. Theory Comput.* **2013**, *9*, 3084–3095.
- (45) Miao, Y.; Sinko, W.; Pierce, L.; Bucher, D.; Walker, R. C.; McCammon, J. A. Improved Reweighting of Accelerated Molecular Dynamics Simulations for Free Energy Calculation. *J. Chem. Theory Comput.* **2014**, *10*, 2677–2689.
- (46) Halgren, T. A. Identifying and characterizing binding sites and assessing druggability. *J. Chem. Inf. Model.* **2009**, *49*, 377–389.
- (47) Halgren, T. A.; Murphy, R. B.; Friesner, R. A.; Beard, H. S.; Frye, L. L.; Pollard, W. T.; Banks, J. L. Glide: a new approach for rapid, accurate docking and scoring. 2. Enrichment factors in database screening. *J. Med. Chem.* **2004**, *47*, 1750–1759.
- (48) Harder, E.; Damm, W.; Maple, J.; Wu, C.; Reboul, M.; Xiang, J. Y.; Wang, L.; Lupyan, D.; Dahlgren, M. K.; Knight, J. L.; Kaus, J. W.; Cerutti, D. S.; Krilov, G.; Jørgensen, W. L.; Abel, R.; Friesner, R. A. OPLS3: A Force Field Providing Broad Coverage of Drug-like Small Molecules and Proteins. *J. Chem. Theory Comput.* **2016**, *12*, 281–296.
- (49) Yang, J.; Lin, X.; Xing, N.; Zhang, Z.; Zhang, H.; Wu, H.; Xue, W. Structure-Based Discovery of Novel Nonpeptide Inhibitors Targeting SARS-CoV-2 M(pro). *J. Chem. Inf. Model.* **2021**, *61*, 3917–3926.
- (50) Wang, E.; Sun, H.; Wang, J.; Wang, Z.; Liu, H.; Zhang, J. Z. H.; Hou, T. End-Point Binding Free Energy Calculation with MM/PBSA and MM/GBSA: Strategies and Applications in Drug Design. *Chem. Rev.* **2019**, *119*, 9478–9508.
- (51) Zhang, Y.; Zheng, G.; Fu, T.; Hong, J.; Li, F.; Yao, X.; Xue, W.; Zhu, F. The binding mode of vilazodone in the human serotonin transporter elucidated by ligand docking and molecular dynamics simulations. *Phys. Chem. Chem. Phys.* **2020**, *22*, S132–S144.
- (52) Tu, G.; Fu, T.; Yang, F.; Yang, J.; Zhang, Z.; Yao, X.; Xue, W.; Zhu, F. Understanding the Polypharmacological Profiles of Triple Reuptake Inhibitors by Molecular Simulation. *ACS Chem. Neurosci.* **2021**, *12*, 2013–2026.
- (53) Zheng, G.; Yang, F.; Fu, T.; Tu, G.; Chen, Y.; Yao, X.; Xue, W.; Zhu, F. Computational characterization of the selective inhibition of

human norepinephrine and serotonin transporters by an escitalopram scaffold. *Phys. Chem. Chem. Phys.* **2018**, *20*, 29513–29527.

(54) Xue, W.; Yang, F.; Wang, P.; Zheng, G.; Chen, Y.; Yao, X.; Zhu, F. What Contributes to Serotonin-Norepinephrine Reuptake Inhibitors' Dual-Targeting Mechanism? The Key Role of Transmembrane Domain 6 in Human Serotonin and Norepinephrine Transporters Revealed by Molecular Dynamics Simulation. *ACS Chem. Neurosci.* **2018**, *9*, 1128–1140.

(55) Xue, W.; Wang, P.; Tu, G.; Yang, F.; Zheng, G.; Li, X.; Li, X.; Chen, Y.; Yao, X.; Zhu, F. Computational identification of the binding mechanism of a triple reuptake inhibitor amitifadine for the treatment of major depressive disorder. *Phys. Chem. Chem. Phys.* **2018**, *20*, 6606–6616.

## Recommended by ACS

### Transformation of a Dopamine D<sub>2</sub> Receptor Agonist to Partial Agonists as Novel Antipsychotic Agents

Ruiquan Liu, Jianjun Cheng, *et al.*

MAY 02, 2023  
JOURNAL OF MEDICINAL CHEMISTRY

READ 

### Dopamine D<sub>3</sub>/D<sub>2</sub> Receptor Ligands Based on Cariprazine for the Treatment of Psychostimulant Use Disorders That May Be Dual Diagnosed with Affective Disorders

Emma S. Gogarnoiu, Amy Hauck Newman, *et al.*

JANUARY 20, 2023  
JOURNAL OF MEDICINAL CHEMISTRY

READ 

### Pharmacological and Physicochemical Properties Optimization for Dual-Target Dopamine D<sub>3</sub> (D<sub>3</sub>R) and $\mu$ -Opioid (MOR) Receptor Ligands as Potentially Safer Ana...

Alessandro Bonifazi, Amy Hauck Newman, *et al.*

JULY 19, 2023  
JOURNAL OF MEDICINAL CHEMISTRY

READ 

### Design, Synthesis, Molecular Docking, and Biological Evaluation of Novel Pimavanserin-Based Analogues as Potential Serotonin 5-HT<sub>2A</sub> Receptor Inverse Agonists

Nader R. Albujuq, Mosa Alsehli, *et al.*

JUNE 28, 2023  
JOURNAL OF MEDICINAL CHEMISTRY

READ 

Get More Suggestions >